


Article

Ni-CeO₂ Catalyst with High Ni Loading Prepared by Salt-Assisted Solution Combustion for CO₂ Methanation

Cui Han ^{1,†}, Zhongqi Cao ^{2,†}, Jiliang Yang ¹, Xinkang Lu ¹, Hui Liu ^{3,*}, Zheyu Jin ⁴, Ying Zhang ², Shuqing Yang ¹, Xianmin Zheng ¹ and Luhui Wang ^{1,5,6,*} 

¹ Zhejiang Key Laboratory of Petrochemical Pollution Control, Zhejiang Ocean University, Zhoushan 316022, China; z19085222012@zjou.edu.cn (C.H.); yjl1997@zjou.edu.cn (J.Y.); lxked@zjou.edu.cn (X.L.); ysqjane@163.com (S.Y.); zheng_xianmin@163.com (X.Z.)

² SINOPEC Dalian Research Institute of Petroleum and Petrochemicals, Dalian 116045, China; caozhongqi.fshy@sinopec.com (Z.C.); zhangying.fshy@sinopec.com (Y.Z.)

³ School of Food and Pharmaceutical, Zhejiang Ocean University, Zhoushan 316022, China

⁴ Department of Chemical and Biological Engineering, School of Engineering, Rensselaer Polytechnic Institute, Troy, NY 12180, USA; jinz6@rpi.edu

⁵ Department of Chemical Engineering, School of Petrochemical Engineering & Environment, Zhejiang Ocean University, Zhoushan 316022, China

⁶ National-Local Joint Engineering Laboratory of Harbor Oil & Gas Storage and Transportation Technology, Zhejiang Ocean University, Zhoushan 316022, China

* Correspondence: liuhui@zjou.edu.cn (H.L.); wangluhui1008@zjou.edu.cn (L.W.); Tel.: +86-580-255-1050 (H.L. & L.W.)

† These authors contributed equally to this work.



Citation: Han, C.; Cao, Z.; Yang, J.; Lu, X.; Liu, H.; Jin, Z.; Zhang, Y.; Yang, S.; Zheng, X.; Wang, L. Ni-CeO₂ Catalyst with High Ni Loading Prepared by Salt-Assisted Solution Combustion for CO₂ Methanation. *Crystals* **2022**, *12*, 702. <https://doi.org/10.3390/cryst12050702>

Academic Editors: Waldemar Maniukiewicz and Younes Hanifehpour

Received: 17 April 2022

Accepted: 13 May 2022

Published: 15 May 2022

Publisher's Note: MDPI stays neutral with regard to jurisdictional claims in published maps and institutional affiliations.



Copyright: © 2022 by the authors. Licensee MDPI, Basel, Switzerland. This article is an open access article distributed under the terms and conditions of the Creative Commons Attribution (CC BY) license (<https://creativecommons.org/licenses/by/4.0/>).

Abstract: An Ni-CeO₂ catalyst with high Ni loading (50 wt.%) prepared by a salt-assisted solution combustion method was characterized by different methods and used for CO₂ methanation. The specific surface area of the Ni-CeO₂ catalyst prepared by salt-assisted solution combustion is 7 times that of the catalyst prepared by conventional solution combustion. The Ni-CeO₂ catalyst prepared by salt-assisted solution combustion has smaller particle sizes of Ni and exhibits excellent activity at low temperatures. The high Ni loading and small Ni particle size can provide more metal Ni site and Ni-CeO₂ interface, which help to improve the CO₂ methanation performance.

Keywords: Ni-CeO₂; CO₂ methanation; salt-assisted solution combustion; high loading

1. Introduction

Excessive emission of carbon dioxide (CO₂) will aggravate the greenhouse effect, and CO₂ conversion has attracted more and more attention. CO₂ methanation is one of the most popular technologies for CO₂ conversion; it is also called the Sabatier reaction [1–3]. CO₂ methanation provides practical ideas for the large-scale conversion of renewable hydrogen to CH₄. CH₄, the product of CO₂ methanation, can be stored in natural gas network facilities.

CO₂ methanation is a reaction in which CO₂ is reduced to CH₄ and subject to kinetic limitations [4–6]. Ru [7], Pd [8], Ni [9], etc., supported on different supports (SiO₂ [8,10], ZrO₂ [11,12], CeO₂ [13,14], etc.), have been investigated for CO₂ methanation. Supported Ni-based catalysts with relatively high activities as well as lower costs have become the most widely studied materials in recent years. In addition, CO₂ methanation is a highly exothermic reaction, so the equilibrium conversion of carbon dioxide will decrease with the increase in reaction temperature [12]. Therefore, it is necessary to develop Ni-based CO₂ methanation catalysts with high activity at low temperature.

Solution combustion methods have made outstanding contributions in the preparation of nanometer material [15,16]. Solution combustion methods have a series of superiorities in the preparation process, such as a relatively simple device, low cost involved, fast reaction

process, and low preheating temperature [17–19]. However, the solution combustion method often results in the shortcoming of a low specific surface area as well as large particle size, which will decrease the catalyst activity.

Salt-assisted solution combustion is a new method to prepare nanomaterials with a high specific surface area, which can overcome the disadvantage of the low specific surface area of nanomaterials prepared by a conventional solution combustion method [20–23]. During combustion, inert salt such as NaCl and KCl can be deposited between nanoparticles, preventing the agglomeration and sintering of the nanoparticles. Then, by dissolving the salt with water or other solvents, nanomaterials with high specific surface areas can be obtained.

CeO₂ has an excellent oxidation-reduction property and is widely used as a support in catalysts, which can inhibit the sintering of metal and minimize carbon deposition [24,25]. The oxygen vacancies in CeO₂ caused by the Ce³⁺/Ce⁴⁺ ion pair make CO₂ effectively activated, and a lot of studies have proved that using CeO₂ can decrease Ni particle size in the catalyst and produce oxygen vacancies, and then the activity of the catalyst is boosted. Ni-CeO₂ catalyst has been reported for CO₂ methanation [26–33]. Ye et al. [29] found that the maximization of the Ni-CeO₂ interface is the key to improve the catalyst activity in the low-temperature CO₂ transformation process, and the Ni embedded into CeO₂ can improve the stability of Ni nanoparticles. At a lower reaction temperature, the enriched Ni-CeO₂ interface and Ni particles with higher dispersity can work synergistically, thus effectively completing the CO₂ methanation process [30,31].

Theoretically, increasing Ni content and decreasing Ni particle size can increase the Ni-Ce interface. However, the existing literature on Ni-CeO₂ catalysts is mainly regarding low Ni-content catalysts. This is because a higher Ni load is often accompanied by a larger Ni particle size, which reduces the catalytic activity.

In this paper, to the best of our knowledge, Ni-CeO₂ (SSC) catalysts with 50% Ni loading were prepared by salt-assisted solution combustion and used for CO₂ methanation for the first time. The salt-assisted solution combustion method can solve the problem of a low specific surface area caused by the conventional solution combustion method and obtain small Ni particles when the catalyst has a higher Ni loading. This enables the catalyst with higher Ni loadings to achieve high activity at low temperatures in the CO₂ methanation reaction.

2. Materials and Methods

2.1. Catalyst Preparation

An Ni-CeO₂(SSC) catalyst with 50 wt.% Ni loading was prepared by a salt-assisted solution combustion method. For salt-assisted solution combustion, Ni(NO₃)₂·6H₂O and Ce(NO₃)₃·6H₂O were added as oxidants, glycine was added as fuel and NaCl as salt. An amount of 2.48 g of Ni(NO₃)₂·6H₂O, 1.26 g of Ce(NO₃)₃·6H₂O, 0.89 g of glycine, and 0.35 g of NaCl were put into beaker and dissolved in 20 mL of deionized water. The beaker was heated at 210 °C until the water evaporated and a combustion reaction took place to produce a solid powder. The solid powder was calcinated at 450 °C for 4 h. After cooling, the sample was washed several times with deionized water to remove NaCl. Silver nitrate solution was used to detect whether there was Cl residue in the washing solution. The Ni-CeO₂ (SSC) catalyst was obtained after drying at 120 °C.

For comparison, the Ni-CeO₂(SC) catalyst with 50 wt.% Ni loading was prepared by a solution combustion method without adding NaCl. In this case, the sample was calcined at 450 °C for 4 h.

The Ni and Na content were determined by atomic absorption spectrophotometer (AAS). The Ni content of the Ni-CeO₂(SSC) and Ni-CeO₂(SC) catalysts was 46.3 wt.% and 48.5 wt.%, respectively, which is close to the theoretical value. The Na residue in the Ni-CeO₂(SSC) catalyst was 0.06 wt.%.

2.2. Catalyst Characterization

Nitrogen adsorption and desorption were measured using an Autosorb-iQ analyzer (Quanta chrome Instruments, Boynton Beach, FL, USA) at $-196\text{ }^{\circ}\text{C}$. The specific surface area was calculated by BET method. The average pore size distribution was obtained from the desorption isotherm using the BJH method.

The X-ray diffraction (XRD) measurements were carried out on a DX-2700 X-ray diffractometer (Haoyuan Instrument, Dandong, China) using $\text{Cu K}\alpha$ radiation. The scanning range of 2θ was from 10° to 80° with a step size of $0.02^{\circ}/1\text{ s}$. The crystallite sizes in the catalysts were obtained with the Scherrer equation.

H_2 temperature programmed reduction (H_2 -TPR) was operated on a multifunctional adsorption instrument TP-5080 (xianquan Industrial and trading Co., Ltd., Tianjin, China), and the instrument was used with a thermal conductivity detection device (TCD). A quartz tube was charged with 50 mg of catalyst and then pretreated with Ar (20 mL/min) at $400\text{ }^{\circ}\text{C}$ for 25 min. After cooling, the reactor was purged using 5% H_2/Ar (20 mL/min) for 0.5 h. Finally, H_2 -TPR tests were performed in 5% H_2/Ar (20 mL/min) from $25\text{ }^{\circ}\text{C}$ to $850\text{ }^{\circ}\text{C}$ ($10\text{ }^{\circ}\text{C}/\text{min}$).

The tested instrument of H_2 temperature programmed desorption (H_2 -TPD) is consistent with H_2 -TPR. First, 50 mg of catalyst was reduced at $450\text{ }^{\circ}\text{C}$ with 5% H_2/Ar (20 mL/min) for 40 min, then it was reduced to $25\text{ }^{\circ}\text{C}$ and adsorbed at $50\text{ }^{\circ}\text{C}$ for 15 min. After being purged with Ar for 1 h, desorption was performed in Ar (20 mL/min) from 30 to $830\text{ }^{\circ}\text{C}$ ($10\text{ }^{\circ}\text{C}/\text{min}$). The specific surface area of Ni was calculated from the amount of H_2 desorption using the assumption that the stoichiometric ratio of $\text{H}/\text{Ni}_{\text{surface}}$ is 1.

TEM measurements were performed on a Tecnai G2 F20 (FEI company, USA) microscope. Before the test, the catalyst powder was evenly dispersed in ethanol after ultrasonic treatment for 30 min, and then the solution was dripped onto the carbon-supported copper mesh by a capillary tube, dried and analyzed.

2.3. Catalyst Performance Test

Catalytic performance tests were performed at atmospheric pressure, and the catalyst was mixed with quartz sand at a ratio of 1:10 and then loaded into a quartz tube reactor (inner diameter is 8 mm, outer diameter is 12 mm, length is 49 cm). The reactor temperature was controlled by a PID temperature controller, and a thermocouple was placed in the middle of catalyst bed. After reduction at $450\text{ }^{\circ}\text{C}$ for 40 min and cooling to $250\text{ }^{\circ}\text{C}$, the reaction was carried out in a gas environment of 40 mL/min of H_2 , 10 mL/min of CO_2 , and 50 mL/min of N_2 . The aging test of the catalysts was carried out at WHSV of $300,000\text{ mL g}^{-1}\text{ h}^{-1}$. The temperature range was $250\text{--}450\text{ }^{\circ}\text{C}$. The outlet gas of the reactor was first condensed and dehydrated, and then analyzed by a PGENERAL G5 on-line gas chromatography. The gas chromatography was equipped with a TCD detector and a TDX-01 column and used H_2 as carrier gas.

CO_2 conversion and CH_4 selectivity are calculated as follows:

$$X_{\text{CO}_2} = \frac{F_{\text{CO}_2,\text{in}} - F_{\text{CO}_2,\text{out}}}{F_{\text{CO}_2,\text{in}}} \times 100\%$$

$$S_{\text{CH}_4} = \frac{F_{\text{CH}_4,\text{out}}}{F_{\text{CO}_2,\text{in}} - F_{\text{CO}_2,\text{out}}} \times 100\%$$

where F is the molar flow rate.

3. Results and Discussion

The nitrogen adsorption/desorption isotherms of $\text{Ni-CeO}_2(\text{SSC})$ and $\text{Ni-CeO}_2(\text{SC})$ catalysts are shown in Figure 1a. From the IUPAC classification, the isotherms showed typical type IV isotherms and hysteresis loops [34], which indicates that the catalyst contains a mesopore structure. Analyzing Figure 1b, the mesoporous structure in the $\text{Ni-CeO}_2(\text{SSC})$ catalyst increased significantly after NaCl was used. As shown in Table 1, the specific

surface area of Ni-CeO₂(SSC) is about 7 times that of the Ni-CeO₂(SC) catalyst, and the pore volume of Ni-CeO₂(SSC) is also higher than that of Ni-CeO₂(SC). Therefore, the addition of NaCl allowed the pore structure of the catalyst to be optimized, while the S_{BET} of the catalyst was greatly increased.

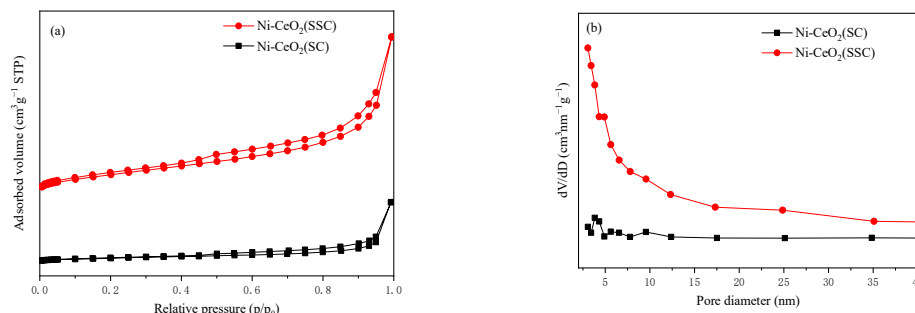


Figure 1. (a) N₂ adsorption/desorption isotherms and pore size distributions (b) of Ni-CeO₂(SSC) and Ni-CeO₂(SC) catalysts.

Table 1. Textural parameters of Ni-CeO₂(SSC) and Ni-CeO₂(SC) catalysts.

Sample	S _{BET} (m ² /g)	Pore Volume (cm ³ /g)	Pore Size (nm)
Ni-CeO ₂ (SC)	11.2	0.07	23.8
Ni-CeO ₂ (SSC)	77.5	0.18	9.9

After the catalyst was reduced at 450 °C for 40 min, XRD tests were performed, and the results are collated in Figure 2. The diffraction peaks at 44° and 51.8° are attributed to metal Ni [35], while others are attributed to CeO₂. The addition of NaCl increases the half peak width of all diffraction peaks. It suggests that the addition of NaCl reduces the particle size of Ni and CeO₂ in the catalyst, and the dispersity of Ni in the catalysts was enhanced. The data in Table 2 about the crystal sizes of catalysts were calculated according to the Scherrer equation [36]. From the data in Table 2, it can be concluded that the Ni and CeO₂ particle sizes of the reduced Ni-CeO₂(SSC) is much smaller than that of the Ni-CeO₂(SC). After NaCl was used, the Ni crystal size decreased from 21.4 nm to 7.2 nm, and the specific surface area of Ni (S_{Ni}) increased from 5.87 to 11.45 m²/g_{cat}. Kang [37] prepared 24 wt.% Ni/CeO₂-HH-2 catalyst with the solution combustion method, and the grain size of Ni reached 23 nm, while the S_{BET} was about 14 m²/g, which is similar to the Ni-CeO₂(SC) in our work.

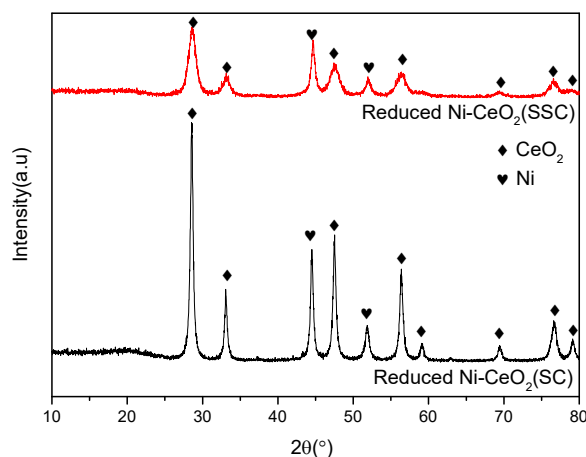


Figure 2. XRD patterns of reduced Ni-CeO₂(SC) and Ni-CeO₂(SSC) catalysts.

Table 2. Crystal sizes and S_{Ni} of reduced Ni-CeO₂(SC) and Ni-CeO₂(SSC) catalysts.

Samples	Ni (nm) ^a	CeO ₂ (nm) ^a	S_{Ni} (m ² /g _{cat}) ^b
Ni-CeO ₂ (SC)	21.4	18.8	5.87
Ni-CeO ₂ (SSC)	7.2	11.2	11.45

^a Calculated from XRD results based on Scherrer's equation. ^b Calculated from H₂-TPD results.

The catalyst reduced at 450 °C for 40 min was characterized by TEM, and the results are shown in Figure 3. As shown in Figure 3a, the particle size of the Ni-CeO₂(SC) catalyst is about 20 nm; large Ni and CeO₂ particles can be found in Figure 3b. By taking the statistics of Figure 3c, the particle size of Ni-CeO₂(SSC) catalysts is about 10 nm. As shown in Figure 3d, the small particles of Ni and CeO₂ are observed to have obvious contact in the Ni-CeO₂(SSC) catalyst. It can be seen in Figure 3e,f that the particle size in the catalyst of Ni-CeO₂(SSC) is far less than Ni-CeO₂(SC). This result is consistent with that obtained by XRD, indicating that the salt-assisted solution combustion method allows the particle size of catalysts to decrease significantly and form a rich metal-support interface.

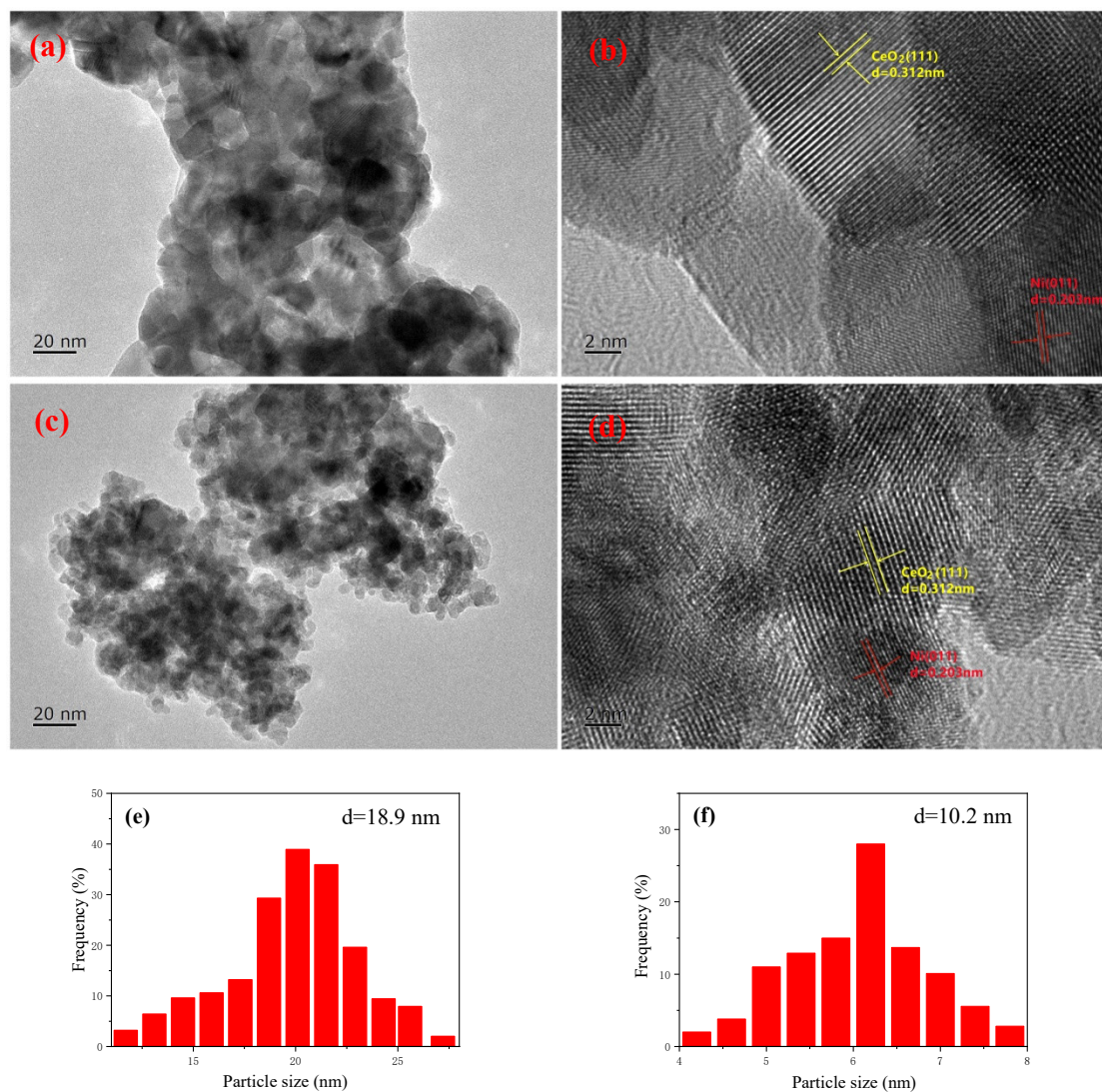
**Figure 3.** TEM images particle size distributions of reduced Ni-CeO₂(SC) (a,b,e) and Ni-CeO₂(SSC) (c,d,f) catalysts.

Figure 4 shows the H₂-TPR spectra of the Ni-CeO₂(SC) and Ni-CeO₂(SSC) catalysts. The Ni-CeO₂(SC) catalyst exhibits a distinct peak centered at 404 °C. Combining the results

of XRD and TEM, this reduction peak should be due to the decrease in bulk NiO. A weak wide peak around 780 °C was caused by the decrease in bulk CeO₂ [38]. The reduction peak for superficial CeO₂ was usually between 400 and 600 °C [39], which should be covered by the peak of NiO.

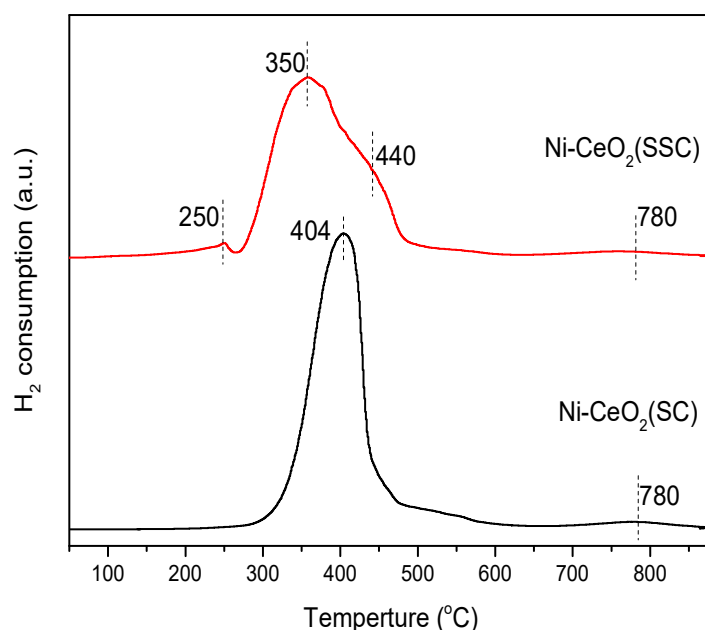


Figure 4. H₂-TPR of Ni-CeO₂(SC) and Ni-CeO₂(SSC) catalysts.

With regard to the Ni-CeO₂(SSC) catalyst, an indistinct reduction peak can be observed at around 250 °C, which is due to the oxygen vacancy generated in Ni_xCe_{1-x}O_y solid solution adsorbing oxygen and reducing it [38]. A few Ni²⁺ ions can enter the CeO₂ crystal lattice to form a Ni_xCe_{1-x}O_y solid solution, and the solid solution causes the generation of oxygen vacancies [38]. Some oxygen is more easily adsorbed into the oxygen vacancy (Ni-V_{ox}-Ce) of the solid solution, which can be reduced to below 300 °C. This indicates that the use of NaCl promotes the generation of the Ni_xCe_{1-x}O_y solid solution. In addition, the oxygen vacancies (Ni-V_{ox}-Ce) in the Ni_xCe_{1-x}O_y solid solution play a huge part in promoting the activity of the CO₂ methanation reaction. The wide reduction peak from 300 to 500 °C belongs to the reduction peak of NiO. Most of the reduction peaks are concentrated at about 350 °C, which is the result of reduction after the weak interaction between highly dispersed NiO and CeO₂, while a slightly wider reduction peak found near 440 °C belongs to the reduction of surface CeO₂, and the highly dispersed NiO strongly interacted with CeO₂ [38]. The reduction of surface CeO₂ is usually between 400 and 600 °C. The TPR results indicate that the salt-assisted solution combustion method makes it easy to form Ni_xCe_{1-x}O_y solid solution in the catalyst; at the same time, the interaction between NiO and CeO₂ was increased.

The performance of the two catalysts was tested for CO₂ methanation. As shown in Figure 5a,b, when the temperature range is 250 to 350 °C, the two groups of catalysts showed similar regularities. The CO₂ conversion of the Ni-CeO₂(SSC) catalyst is much higher than that of the Ni-CeO₂(SC) catalyst. At 400 °C, the CH₄ selectivity of the two catalysts began to decrease (as shown in Figure 5b), which was due to the emergence of a small amount of CO from the reverse water-gas shift reaction at high temperature. Especially when the temperature was at 250 °C, the CO₂ conversion (9.9%) of Ni-CeO₂(SSC) was about 3 times the CO₂ conversion (3.4%) of Ni-CeO₂(SC).

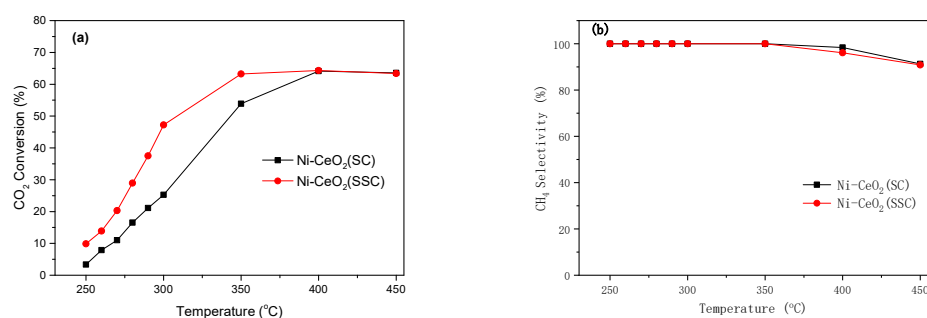


Figure 5. CO₂ methanation over Ni-CeO₂(SC) and Ni-CeO₂(SSC) catalysts: (a) CO₂ conversion, (b) CH₄ selectivity (reaction condition: P = 1.0 bar, WHSV = 300,000 mL g^{−1} h^{−1}, n(CO₂):n(H₂):n(N₂) = 1:4:5).

Figure 6 shows the CO₂ conversion during the stability test of Ni-CeO₂ (SSC) at 350 °C for 50 h. The sample shows high stability, and the carbon dioxide conversion rate is only reduced by 6.2% within 50 h. This could be due to the interaction between the small Ni and CeO₂ particles, which can prevent the nickel particles from sintering during the reaction.

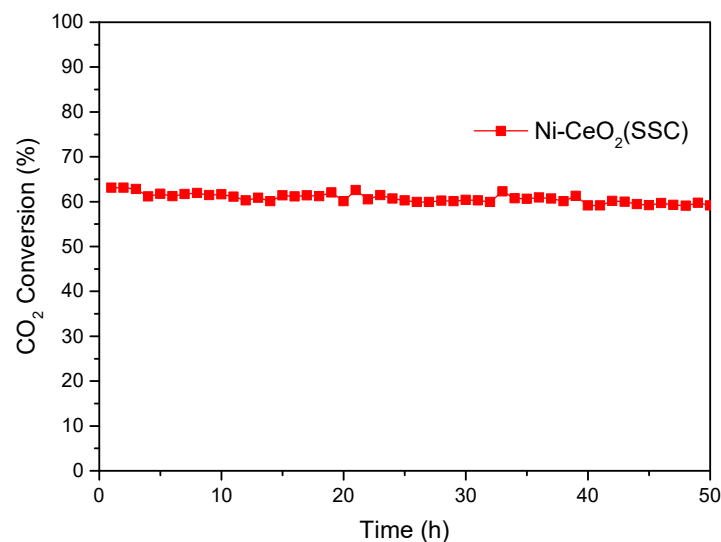


Figure 6. The stability of the Ni-CeO₂(SSC) catalyst (reaction condition: T = 350 °C, P = 1.0 bar, WHSV = 300,000 mL g^{−1} h^{−1}, n(CO₂):n(H₂):n(N₂) = 1:4:5).

According to the performance test and characterization results of the catalysts, it can be seen that the salt-assisted solution combustion method can significantly improve the specific surface area and reduce the metal and support particle sizes of the high metal loading Ni-CeO₂ catalyst, while facilitating the formation of oxygen vacancies (Ni-V_{ox}-Ce), thus improving the activity of the catalyst. The small Ni particle size provides more metallic Ni surface for adsorption and activation of hydrogen, which then can react with CO₂ adsorbed on CeO₂ to form CH₄. The enriched Ni-CeO₂ interface makes it easier for adsorbed hydrogen to react with adsorbed CO₂. Rui et al. [30] found that the abundant Ni-CeO₂ interfacial sites had more excellent activity than the inert lattice oxygen atoms in CeO₂. Tada et al. [31] reported that the CO₂ conversion rate had no direct connection with the number of oxygen vacancies on CeO₂ (Ce-V_{ox}-Ce) but was affected by the number of Ni-V_{ox}-Ce sites.

4. Conclusions

The Ni-CeO₂(SSC) catalyst with a high Ni loading of 50 wt.% prepared by a salt-assisted solution combustion method exhibits a high CO₂ conversion rate in CO₂ metha-

nation. Compared with the Ni-CeO₂(SC) catalyst, the Ni-CeO₂(SSC) catalyst has a larger specific surface area and smaller Ni particle size, and thus has a rich metal surface and metal-support interface, so it has good performance in methanation reactions. A salt-assisted solution combustion method can overcome the problems of particle sintering and low specific surface area caused by the traditional solution combustion method and provides a simple strategy for the preparation of high metal loading and high dispersed metal catalyst.

Author Contributions: Conceptualization, L.W.; data curation, C.H.; formal analysis, C.H., Z.C., J.Y., X.L., Z.J. and Y.Z.; funding acquisition, Z.C. and L.W.; investigation, C.H. and L.W.; writing—original draft, C.H., H.L. and L.W.; writing—review and editing, S.Y., X.Z. and L.W. All authors have read and agreed to the published version of the manuscript.

Funding: This research was funded by the Science and Technology Foundation of Zhoushan (No. 2022C41002) and SINOPEC (No. 112109).

Institutional Review Board Statement: Not applicable.

Informed Consent Statement: Not applicable.

Data Availability Statement: Not applicable.

Conflicts of Interest: The authors declare no conflict of interest.

References

- Nie, W.; Zou, X.; Shang, X.; Wang, X.; Ding, W.; Lu, X. CeO₂-assisted Ni nanocatalysts supported on mesoporous γ -Al₂O₃ for the production of synthetic natural gas. *Fuel* **2017**, *202*, 135–143. [CrossRef]
- Wang, W.; Wang, S.; Ma, X.; Gong, J. Recent advances in catalytic hydrogenation of carbon dioxide. *Chem. Soc. Rev.* **2011**, *40*, 3703–3727. [CrossRef] [PubMed]
- Pandey, D.; Ray, K.; Bhardwaj, R.; Bojja, S.; Chary, K.; Deo, G. Promotion of unsupported nickel catalyst using iron for CO₂ methanation. *Int. J. Hydrog. Energy* **2018**, *43*, 4987–5000. [CrossRef]
- Biset-Peiró, M.; Guílera, J.; Zhang, T.; Arbiol, J.; Andreu, T. On the role of ceria in Ni-Al₂O₃ catalyst for CO₂ plasma methanation. *Appl. Catal. A Gen.* **2019**, *575*, 223–229. [CrossRef]
- Xu, J.; Su, X.; Duan, H.; Hou, B.; Lin, Q.; Liu, X.; Pan, X.; Pei, G.; Geng, H.; Huang, Y. Influence of pretreatment temperature on catalytic performance of rutile TiO₂-supported ruthenium catalyst in CO₂ methanation. *J. Catal.* **2016**, *333*, 227–237. [CrossRef]
- Su, X.; Xu, J.; Liang, B.; Duan, H.; Hou, B.; Huang, Y. Catalytic carbon dioxide hydrogenation to methane: A review of recent studies. *J. Energy Chem.* **2016**, *25*, 553–565. [CrossRef]
- Wang, F.; He, S.; Chen, H.; Wang, B.; Zheng, L.; Wei, M.; Evans, D.G.; Duan, X. Active site dependent reaction mechanism over Ru/CeO₂ catalyst toward CO₂ methanation. *J. Am. Chem. Soc.* **2016**, *138*, 6298–6305. [CrossRef]
- Kim, H.Y.; Lee, H.M.; Park, J.-N. Bifunctional mechanism of CO₂ methanation on Pd-MgO/SiO₂ catalyst: Independent roles of MgO and Pd on CO₂ methanation. *J. Phys. Chem. C* **2010**, *114*, 7128–7131. [CrossRef]
- Wei, W.; Jinlong, G. Methanation of carbon dioxide: An overview. *Front. Chem. Sci. Eng.* **2011**, *5*, 2–10. [CrossRef]
- Aziz, M.; Jalil, A.; Triwahyono, S.; Mukti, R.; Taufiq-Yap, Y.; Sazegar, M. Highly active Ni-promoted mesostructured silica nanoparticles for CO₂ methanation. *Appl. Catal. B Environ.* **2014**, *147*, 359–368. [CrossRef]
- Zhao, K.; Wang, W.; Li, Z. Highly efficient Ni/ZrO₂ catalysts prepared via combustion method for CO₂ methanation. *J. CO₂ Util.* **2016**, *16*, 236–244. [CrossRef]
- Tan, J.; Wang, J.; Zhang, Z.; Ma, Z.; Wang, L.; Liu, Y. Highly dispersed and stable Ni nanoparticles confined by MgO on ZrO₂ for CO₂ methanation. *Appl. Surf. Sci.* **2019**, *481*, 1538–1548. [CrossRef]
- Atzori, L.; Cutrufello, M.G.; Meloni, D.; Cannas, C.; Gazzoli, D.; Monaci, R.; Sini, M.F.; Rombi, E. Highly active NiO-CeO₂ catalysts for synthetic natural gas production by CO₂ methanation. *Catal. Today* **2018**, *299*, 183–192. [CrossRef]
- Ge, Y.; He, T.; Han, D.; Li, G.; Zhao, R.; Wu, J. Plasma-assisted CO₂ methanation: Effects on the low-temperature activity of an Ni-Ce catalyst and reaction performance. *R. Soc. Open Sci.* **2019**, *6*, 190750. [CrossRef] [PubMed]
- Varma, A.; Mukasyan, A.S.; Rogachev, A.S.; Manukyan, K.V. Solution Combustion Synthesis of Nanoscale Materials. *Chem. Rev.* **2016**, *116*, 14493–14586. [CrossRef] [PubMed]
- Carlos, E.; Martins, R.; Fortunato, E.; Branquinho, R. Solution combustion synthesis: Towards a sustainable approach for metal oxides. *Chem.—A Eur. J.* **2020**, *26*, 9099–9125. [CrossRef] [PubMed]
- Cross, A.; Roslyakov, S.; Manukyan, K.V.; Rouvimov, S.; Rogachev, A.S.; Kovalev, D.; Wolf, E.E.; Mukasyan, A.S. In situ preparation of highly stable Ni-based supported catalysts by solution combustion synthesis. *J. Phys. Chem. C* **2014**, *118*, 26191–26198. [CrossRef]
- Ullah, N.; Qu, J.; Li, Z. Enhanced sulfur-resistant methanation performance over MoO₃-ZrO₂ catalyst prepared by solution combustion method. *Appl. Organomet. Chem.* **2019**, *33*, e5022.

19. Jiang, Y.; Huang, T.; Dong, L.; Qin, Z.; Ji, H. Ni/bentonite catalysts prepared by solution combustion method for CO₂ methanation. *Chin. J. Chem. Eng.* **2018**, *26*, 2361–2367. [\[CrossRef\]](#)
20. Abbasian, A.R.; Mahvary, A.; Alirezaei, S. Salt-assisted solution combustion synthesis of NiFe₂O₄: Effect of salt type. *Ceram. Int.* **2021**, *47*, 23794–23802. [\[CrossRef\]](#)
21. Chen, W.; Li, F.; Yu, J.; Liu, L. A facile and novel route to high surface area ceria-based nanopowders by salt-assisted solution combustion synthesis. *Mater. Sci. Eng. B* **2006**, *133*, 151–156. [\[CrossRef\]](#)
22. Abbasian, A.R.; Rahmani, M. Salt-assisted solution combustion synthesis of nanostructured ZnFe₂O₄-ZnS powders. *Inorg. Chem. Commun.* **2020**, *111*, 107629. [\[CrossRef\]](#)
23. Zhao, Y.; Jiang, N.; Zhang, X.; Guo, J.; Yang, Q.; Gao, L.; Li, Y.; Ma, T. One-step salt-assisted solution combustion synthesis of Ni-based composites for use as supercapacitor electrodes. *J. Alloy. Compd.* **2018**, *765*, 396–404. [\[CrossRef\]](#)
24. Zhou, G.; Liu, H.; Cui, K.; Jia, A.; Hu, G.; Jiao, Z.; Liu, Y.; Zhang, X. Role of surface Ni and Ce species of Ni/CeO₂ catalyst in CO₂ methanation. *Appl. Surf. Sci.* **2016**, *383*, 248–252. [\[CrossRef\]](#)
25. Guo, Y.; Zou, J.; Shi, X.; Rukundo, P.; Wang, Z.-j. A Ni/CeO₂-CDC-SiC catalyst with improved coke resistance in CO₂ reforming of methane. *ACS Sustain. Chem. Eng.* **2017**, *5*, 2330–2338. [\[CrossRef\]](#)
26. Zhou, G.; Liu, H.; Cui, K.; Xie, H.; Jiao, Z.; Zhang, G.; Xiong, K.; Zheng, X. Methanation of carbon dioxide over Ni/CeO₂ catalysts: Effects of support CeO₂ structure. *Int. J. Hydrog. Energy* **2017**, *42*, 16108–16117. [\[CrossRef\]](#)
27. Tada, S.; Shimizu, T.; Kameyama, H.; Haneda, T.; Kikuchi, R. Ni/CeO₂ catalysts with high CO₂ methanation activity and high CH₄ selectivity at low temperatures. *Int. J. Hydrog. Energy* **2012**, *37*, 5527–5531. [\[CrossRef\]](#)
28. Tada, S.; Ikeda, S.; Shimoda, N.; Honma, T.; Takahashi, M.; Nariyuki, A.; Satokawa, S. Sponge Ni catalyst with high activity in CO₂ methanation. *Int. J. Hydrog. Energy* **2017**, *42*, 30126–30134. [\[CrossRef\]](#)
29. Ye, R.-P.; Li, Q.; Gong, W.; Wang, T.; Razink, J.J.; Lin, L.; Qin, Y.-Y.; Zhou, Z.; Adidharma, H.; Tang, J. High-performance of nanostructured Ni/CeO₂ catalyst on CO₂ methanation. *Appl. Catal. B Environ.* **2020**, *268*, 118474. [\[CrossRef\]](#)
30. Rui, N.; Zhang, X.; Zhang, F.; Liu, Z.; Cao, X.; Xie, Z.; Zou, R.; Senanayake, S.D.; Yang, Y.; Rodriguez, J.A. Highly active Ni/CeO₂ catalyst for CO₂ methanation: Preparation and characterization. *Appl. Catal. B Environ.* **2021**, *282*, 119581. [\[CrossRef\]](#)
31. Tada, S.; Nagase, H.; Fujiwara, N.; Kikuchi, R. What are the best active sites for CO₂ methanation over Ni/CeO₂? *Energy Fuels* **2021**, *35*, 5241–5251. [\[CrossRef\]](#)
32. Lee, S.M.; Lee, Y.H.; Moon, D.H.; Ahn, J.Y.; Nguyen, D.D.; Chang, S.W.; Kim, S.S. Reaction mechanism and catalytic impact of Ni/CeO_{2-x} catalyst for low-temperature CO₂ methanation. *Ind. Eng. Chem. Res.* **2019**, *58*, 8656–8662. [\[CrossRef\]](#)
33. Atzori, L.; Cutrufello, M.G.; Meloni, D.; Monaci, R.; Cannas, C.; Gazzoli, D.; Sini, M.F.; Deiana, P.; Rombi, E. CO₂ methanation on hard-templated NiO-CeO₂ mixed oxides. *Int. J. Hydrog. Energy* **2017**, *42*, 20689–20702. [\[CrossRef\]](#)
34. Kloetstra, K.; Zandbergen, H.; Van Koten, M.; Van Bekkum, H. Thermoporometry as a new tool in analyzing mesoporous MCM-41 materials. *Catal. Lett.* **1995**, *33*, 145–156. [\[CrossRef\]](#)
35. Ocampo, F.; Louis, B.; Roger, A.-C. Methanation of carbon dioxide over nickel-based Ce_{0.72}Zr_{0.28}O₂ mixed oxide catalysts prepared by sol-gel method. *Appl. Catal. A Gen.* **2009**, *369*, 90–96. [\[CrossRef\]](#)
36. Holzwarth, U.; Gibson, N. The Scherrer equation versus the ‘Debye-Scherrer equation’. *Nat. Nanotechnol.* **2011**, *6*, 534. [\[CrossRef\]](#)
37. Kang, W.; Varma, A. Hydrogen generation from hydrous hydrazine over Ni/CeO₂ catalysts prepared by solution combustion synthesis. *Appl. Catal. B Environ.* **2018**, *220*, 409–416. [\[CrossRef\]](#)
38. Shan, W.; Luo, M.; Ying, P.; Shen, W.; Li, C. Reduction property and catalytic activity of Ce_{1-x}Ni_xO₂ mixed oxide catalysts for CH₄ oxidation. *Appl. Catal. A Gen.* **2003**, *246*, 1–9. [\[CrossRef\]](#)
39. Liu, H.; Zhao, C.; Wang, L. Mesoporous Ni-CeO₂ Catalyst with Enhanced Selectivity and Stability for Reverse Water-Gas Shift Reaction. *J. Chem. Eng. Jpn.* **2018**, *49*, 161–165. [\[CrossRef\]](#)